



DESIGN AND OPTIMIZATION OF LATTICE STRUCTURES FOR AEROSPACE APPLICATIONS

Enrico Stragiotti

François-Xavier Irisarri¹, Cédric Julien¹ and Joseph Morlier²

1: ONERA - The French Aerospace Lab
DMAS - Département matériaux et structures
92320 Châtillon, France
{francois-xavier.irisarri, cedric.julien}@onera.fr

2: ICA - Institut Clément Ader
ISAE - SUPAERO
31400 Toulouse, France
joseph.morlier@isae-supraero.fr
December 18, 2023

PhD manuscript

ONERA – ISAE Supaero

Colophon

This document was typeset with the help of KOMA-Script and L^AT_EX using the kaobook class.

ONERA – ISAE Supaero

CONTENTS

Contents	iii
List of Figures	v
List of Tables	v
List of Abbreviations	v
1. Optimizing the layout of the modules in space	1
1.1. Optimize the modules' layout using a modified DMO algorithm	1
1.1.1. Definition of the subdomains cross-sectional areas	1
1.1.2. Variables penalization schemes	2
1.1.3. The optimization formulation and resolution algorithm	3
1.1.4. Optimization initialization: a clustering algorithm to identify similarly behaving subdomains	6
1.2. Numerical application	7
1.2.1. Layout optimization of fixed modules	8
1.2.2. Modules and layout optimization	11
1.2.3. A benchmark case study: a simply supported modular bridge	13
1.2.4. Simply supported 3D beam	18
1.3. Conclusion	19
Bibliography	21
Appendix	23
A. Sensitivity analysis of the modular structure optimization algorithm	25

LIST OF FIGURES

1.1.	2
1.2.	3
1.3.	6
1.4.	7
1.5.	Boundary conditions of the 2D cantilever beam divided in 24x12 subdomains. In the upper part of the image the ground structure of the module composed of $\bar{n} = 6$ elements.	8
1.6.	$V = 832.848$	9
1.7.	$V = 9832.935$	9
1.8.	10
1.9.	11
1.10.	11
1.11.	12
1.12.	12
1.13.	13
1.14.	$V = 1727.314$	13
1.15.	Bailey bridge placed on construction site road over Orava river (Slovakia) [10].	13
1.16.	14
1.17.	15
1.18.	16
1.19.	17
1.20.	17
1.21.	18
1.22.	Symmetric boundary conditions of the simply supported 3D beam. In gray are the symmetry planes of the test case.	18
1.23.	19
1.24.	Perspective view of the monolithic simply supported 3D beam optimized structure with $V = 9.907 \text{ cm}^3$	19

LIST OF TABLES

1.1.	Material data used for the 2D cantilever beam 2D.	8
1.2.	12
1.3.	Material data used for the	14
1.4.	Material data used for the	16
1.5.	Material data used for the simply supported 3D beam optimization.	18
1.6.	19

LIST OF ABBREVIATIONS

DMO	Discrete Material Optimization
FEA	Finite Element Analysis
NLP	Non-Linear Programming
RAMP	Rational Approximation of Material Properties
SIMP	Solid Isotropic Material with Penalization Method

OPTIMIZING THE LAYOUT OF THE MODULES IN SPACE

1

Chapter ?? introduced the basic concept of modular structures and . Additionally it conducted a design of experiments that helped us understand the general mechanical behaviour of modular structures. However we saw that especially the volume of such structure is very penalized if the structure is

1.1 OPTIMIZE THE MODULES' LAYOUT USING A MODIFIED DMO ALGORITHM	1
1.2 NUMERICAL APPLICATION	7
1.3 CONCLUSION	19

1.1. OPTIMIZE THE MODULES' LAYOUT USING A MODIFIED DMO ALGORITHM

The objective of this study is to address the concurrent optimization of both the layout and topology of multiple modules within a modular structure. The key scientific challenge lies in the discrete nature of the layout optimization problem i.e. find the optimal distribution of the different modules within the subdomains of the structure, an inherently discrete problem. Given our intent to employ a gradient descent algorithm [1], it is imperative to design a methodology for converting the discrete nature of the problem into a continuous one, permitting the application of gradient-based optimization techniques.

1. Sigmund (2011), 'On the usefulness of non-gradient approaches in topology optimization'

1.1.1. DEFINITION OF THE SUBDOMAINS CROSS-SECTIONAL AREAS

In this study, our strategy for addressing the discrete layout problem of modules as a continuous one involves defining the variables of the subdomains (i.e., the structure's variables) as a weighted sum of the module variables. This approach draws inspiration from the seminal work of Stegmann and Lund in the Discrete Material Optimization (DMO) algorithm [2], where an optimizer selects the optimal homogenized stiffness tensor for each subdomain from a set of fixed tensors to minimize the compliance of a given structure. In the scenario of discretizing a ground structure into N_{sub} subdomains and utilizing N_T distinct modules, the cross-sectional areas of subdomain j are then expressed as:

$$\bar{\mathbf{a}}^j = \sum_{t=1}^{N_T} w_t^j \bar{\mathbf{a}}_t \quad (1.1)$$

where $\bar{\mathbf{a}}_t$ represent the vector of cross-sectional areas of the t module and w^j is the vector of weight relatives to the j subdomain, defined as $w^j \in \mathbb{R}^t \mid w_j^t \in [0, 1]$.

2. Stegmann et al. (2005), 'Discrete material optimization of general composite shell structures'

An example of a cantilever beam with $N_{\text{sub}} = 8$ and $N_T = 3$ is illustrated in Fig. 1.1, in which we visually demonstrate the impact of modifying the weight values w on the structure topology.

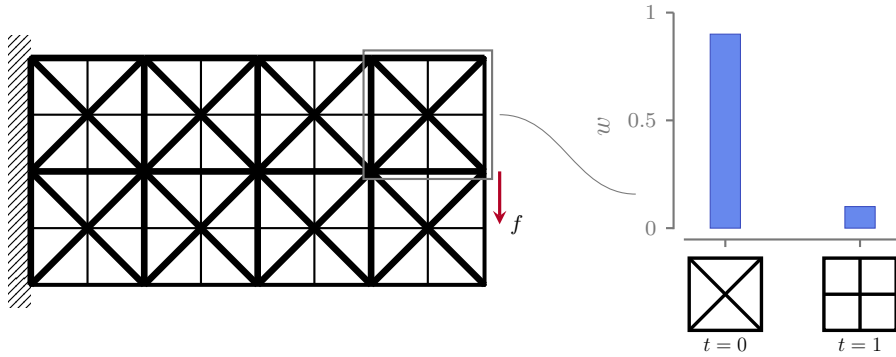


Figure 1.1.

1.1.2. VARIABLES PENALIZATION SCHEMES

The inherent limitation of the proposed approach is that, when the optimizer converges to a solution, the weights of all subdomains must converge to either zero or one, with the additional constraint that only one weight per subdomain can be equal to one. This is necessary to avoid intermediate weights, which would imply a combination of multiple modules' topologies lacking mechanical significance and proving impractical for manufacturing. To address this issue, we implement an interpolation scheme that penalizes intermediate weights. Specifically, we opt for the Rational Approximation of Material Properties (RAMP) method [3] instead of the more commonly used Solid Isotropic Material with Penalization Method (SIMP) interpolation scheme. This choice is motivated by RAMP's advantageous property of ensuring that the derivative is never infinite nor zero when approaching a value of zero.

We define the design variable $\alpha \in \mathbb{R}^{j,t}$ as the modules' layout variable, responsible for the module choice within the subdomain j . Its relationship with the weight w is as follows:

$$w_t^j = \frac{\alpha_t^j}{1 + p(1 - \alpha_t^j)} \quad (1.2)$$

3. Stolpe et al. (2001), 'An alternative interpolation scheme for minimum compliance topology optimization'

4. Hvejsel et al. (2011), 'Material interpolation schemes for unified topology and multi-material optimization'

where $p \in \mathbb{R}^+$ denotes a parameter governing the steepness of the RAMP interpolation. Drawing inspiration from the works of [4], we introduce a multi-phase variant of the RAMP interpolation, in which we concurrently penalize mechanical properties while artificially increasing the volume of modules with intermediate densities. To achieve this, we introduce an additional RAMP parameter, q , always negative ($q \in \mathbb{R}^-$), utilized to assess the augmented weights associated with the volume evaluation V . We can then write:

$$V = \sum_{j=1}^{N_{\text{sub}}} \bar{\ell}^T \tilde{\alpha}^j, \quad (1.3)$$

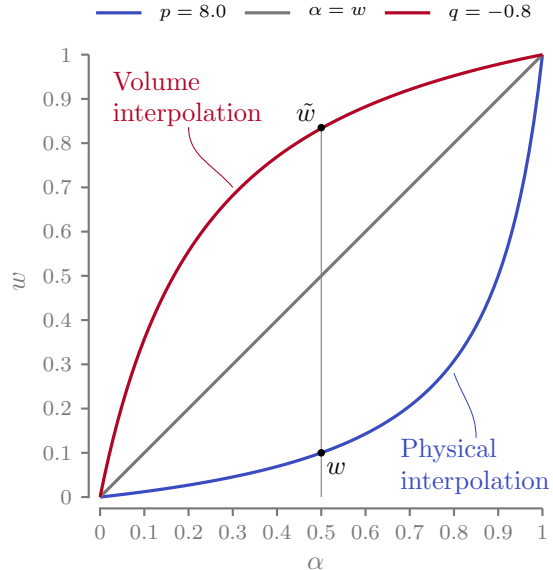


Figure 1.2.

where the vector $\tilde{\mathbf{a}}^j$, representing the increases in cross-sectional areas of the j -th subdomain is defined as following:

$$\tilde{\mathbf{a}}^j = \sum_{t=1}^{N_T} \tilde{w}_t^j \bar{\mathbf{a}}_t, \quad (1.4)$$

and where \tilde{w} is:

$$\tilde{w}_t^j = \frac{\alpha_t^j}{1 + q(1 - \alpha_t^j)}. \quad (1.5)$$

So for every design variable α , we associate two different weights (w and \tilde{w}) that are used to evaluate the mechanical properties and the structure volume, respectively (see Fig. 1.2).

1.1.3. THE OPTIMIZATION FORMULATION AND RESOLUTION ALGORITHM

The objective function of the optimization process is the volume minimization of the modular structure. The members of the structure are subject to multiple mechanical constraints, namely stress, topological buckling, minimum slenderness, and compatibility constraints. Formulation M_1 is stated in terms of modules' cross-sectional area $\bar{\mathbf{a}}$, module selection variables α , member forces q , and nodal

displacements \mathbf{U} as follows:

$$\begin{aligned}
 \min_{\tilde{\mathbf{a}}, \alpha, q, \mathbf{U}} \quad & V = \sum_{j=1}^{N_{\text{sub}}} \tilde{\ell}^T \tilde{\mathbf{a}}^j \quad (\text{Volume minimization}) \\
 \text{s.t.} \quad & \mathbf{Bq} = \mathbf{f} \quad (\text{Force equilibrium}) \\
 & \mathbf{q} = \frac{\mathbf{aE}}{\ell} \mathbf{b}^T \mathbf{U} \quad (\text{Compatibility constraints}) \\
 & \mathbf{q} \geq -\frac{s\mathbf{a}^2}{\ell^2} \quad (\text{Euler buckling constraints}) \quad (\mathbb{M}_1) \\
 & -\sigma_C \mathbf{a} \leq \mathbf{q} \leq \sigma_T \mathbf{a} \quad (\text{Stress constraints}) \\
 & \bar{\mathbf{a}}_{t,r} \geq \bar{\mathbf{a}}_{t,r=1} \quad r \in \mathcal{C}_{l,r}(\bar{\mathbf{a}}_t), \forall t \\
 & 0 \leq \bar{\mathbf{a}} \leq \frac{4\pi\tilde{\ell}^2}{\lambda_{\max}} \quad (\text{Slenderness limit}) \\
 & \sum_{t=1}^{N_T} \alpha_t^j \leq 1, \forall j \quad (\text{One selected module max.})
 \end{aligned}$$

This formulation builds on the classic DMO approach, adding multiple mechanical constraints and while operating on a ground structure. Additionally, we are not only selecting the best module for every subdomain by changing the value of α as classic DMO does, but we are also optimizing the modules' topology simultaneously. This simultaneous optimization presents a more challenging task. The advantages of this formulation lie in dealing with a discrete problem using continuous design variables and a gradient-based optimizer. However, it comes with the drawback of increasing the problem size, as we are adding numerous additional design variables α that scale with the number of subdomains and the number of modules i.e. a vector of size $\alpha^j \in \mathbb{R}^t$ is defined for every one of the j subdomains.

The design variables α are constrained by a set of constraints that limit the maximum sum of α of a submodule j to be less than or equal to one. It is crucial to note that we treat this constraint as a disequality constraint rather than an equality. This allows the optimizer to set all α to zero, permitting the removal of the subdomain from the structure. The constraint is expressed as follows:

$$\sum_{t=1}^{N_T} \alpha_t^j \leq 1, \forall j \quad (1.6)$$

Problem \mathbb{M}_1 is tackled using a modified version of the proposed two-step solving algorithm. In this approach, we initially solve a relaxed problem denoted as \mathbb{M}_2 , where kinematic compatibility constraints are omitted. This relaxed problem is inherently nonlinear due to the introduction of the α design variables. For this iteration, we have chosen to solve it in this form without linearizing the buckling constraints.

The relaxed formulation \mathbb{M}_2 , expressed in terms of modules' cross-sectional area $\bar{\alpha}$, module selection variables α , and member forces q , is the following:

$$\begin{aligned}
 \min_{\bar{\alpha}, \alpha, q} \quad & V = \sum_{j=1}^{N_{\text{sub}}} \bar{\ell}^T \bar{\alpha}^j \quad (\text{Volume minimization}) \\
 \text{s.t.} \quad & Bq = f \quad (\text{Force equilibrium}) \\
 & q \geq -\frac{sa^2}{\ell^2} \quad (\text{Euler buckling constraints}) \\
 & -\sigma_C \alpha \leq q \leq \sigma_T \alpha \quad (\text{Stress constraints}) \\
 & 0 \leq \bar{\alpha} \leq \frac{4\pi\bar{\ell}^2}{\lambda_{\max}} \quad (\text{Slenderness limit}) \\
 & \sum_{t=1}^{N_T} \alpha_t^j \leq 1, \forall j \quad (\text{One selected module max.})
 \end{aligned} \tag{\mathbb{M}_2}$$

Problem \mathbb{M}_2 is solved using a non-linear gradient-based optimizer that iteratively exploits first and second-order derivatives to achieve convergence. The computation of the Jacobian and Hessian matrices for this problem is not trivial, and the details are elaborated in Appendix A.

Once problem \mathbb{M}_2 is solved, we prepare for the second step in which the kinematic compatibility constraints are added again. We exploit the optimized module layout α^* to set up the fixed module layout on the structure, and evaluate the mapping matrix H used in the variable linking approach of problem $\mathbb{M}_{1,\text{VL}}$. The indexes of the mapping matrix H are evaluated as follows:

$$h_{j,t} = \begin{cases} 1 & \text{if } \alpha_{j,t}^* = \max(\alpha_j^*) \text{ and } \alpha_{j,t}^* > 0.01 \\ 0 & \text{otherwise.} \end{cases} \tag{1.7}$$

Subsequently, the compatibility constraints are reintroduced, and a Finite Element Analysis (FEA) is conducted to evaluate the displacements \mathbf{U} used in the starting point of the following optimization step. To mitigate the risk of becoming trapped in local minima, the second step is solved on a reduced design space. The solution $\bar{\alpha}^*$ of the first optimization is used to simplify the initial ground structure, thereby eliminating elements from the optimization that fall below the specified threshold value a_{thr} :

$$\bar{\alpha}_i < a_{\text{thr}} \quad \forall i, \text{ with } a_{\text{thr}} = \chi \max(\bar{\alpha}^*), \tag{1.8}$$

with the parameter χ is the cross-sectional area threshold value.

Now, with all the components in place, we can set up the variable linking formulation $\mathbb{M}_{1,\text{VL}}$, as defined in Chapter ???. This formulation is employed to optimize modular structures with a fixed modules' layout and provide the final optimized design.

Formulation $\mathbb{M}_{1,\text{VL}}$, defined in Chapter ?? permits to optimize modular structures with fixed module layout using the variable linking approach. It is stated in terms of modular cross-sectional areas $\bar{\alpha}$, member forces q and nodal displacements \mathbf{U} as follows:

$$\begin{aligned}
 \min_{\bar{\alpha}, q, U} \quad & V = \ell^T \alpha \\
 \text{s.t.} \quad & \alpha = \sum_{t=1}^{N_T} h_t \otimes \bar{\alpha}_t \\
 & Bq = f \\
 & q = \frac{aE}{\ell} b^T \mathbf{U} \\
 & q \geq -\frac{sa^2}{\ell^2} \\
 & -\sigma_C \alpha \leq q \leq \sigma_T \alpha \\
 & \bar{\alpha}_{t,r} \geq \bar{\alpha}_{t,r=1} \\
 & 0 \leq \bar{\alpha} \leq \frac{4\pi\bar{\ell}^2}{\lambda_{\max}},
 \end{aligned}$$

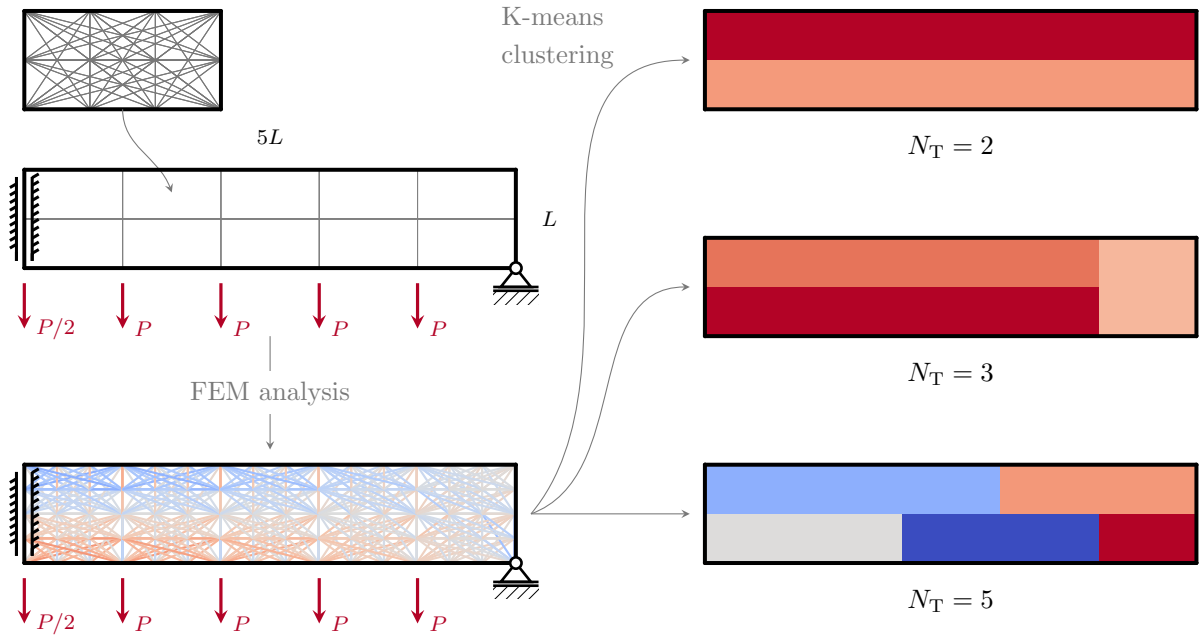


Figure 1.3.

1.1.4. OPTIMIZATION INITIALIZATION: A CLUSTERING ALGORITHM TO IDENTIFY SIMILARLY BEHAVING SUBDOMAINS

In the proposed optimization formulation, we not only adjust the design variables responsible for the modules' layout (α) but also optimize the modules' topology (\bar{a}). However, a significant challenge arises in this problem due to the strong interdependence between the layout and the module topology i.e. the topology of the module is optimized in function of the layout and *vice versa*. It becomes particularly challenging for a gradient-based optimizer to determine the appropriate direction to follow, especially when starting from a completely uniform initial point (as observed in the work of [5]). To mitigate this challenge, we provide a slightly influenced starting point for the optimization process. In this work, we influence the module topology design variable at iteration zero $\alpha_{it} = 0$ as follows:

$$\alpha_{t,init}^j = \begin{cases} \frac{1}{N_T} \cdot 1.1 & \text{if the } j\text{-th subdomain has the } t\text{-th module selected,} \\ \frac{N_T-1.1}{N_T(N_T-1)} & \text{otherwise.} \end{cases} \quad (1.9)$$

5. Bakker et al. (2021), 'Simultaneous optimization of topology and layout of modular stiffeners on shells and plates'

The idea behind how to select the best module for a subdomain is to identify subdomains that show similar mechanical behavior, grouping them based on their stress state. This grouping is assessed using a k-means clustering technique with the number of clusters equal to the number of module topologies, N_T . Given a set of observations $(x_1, x_2, \dots, x_{N_{\text{sub}}})$, where each observation is a \bar{n} -dimensional real vector, k-means clustering aims to partition the N_{sub} observations into N_T sets. In our context, each observation is the vector containing the Finite Element Analysis (FEA) calculated stress distribution on the

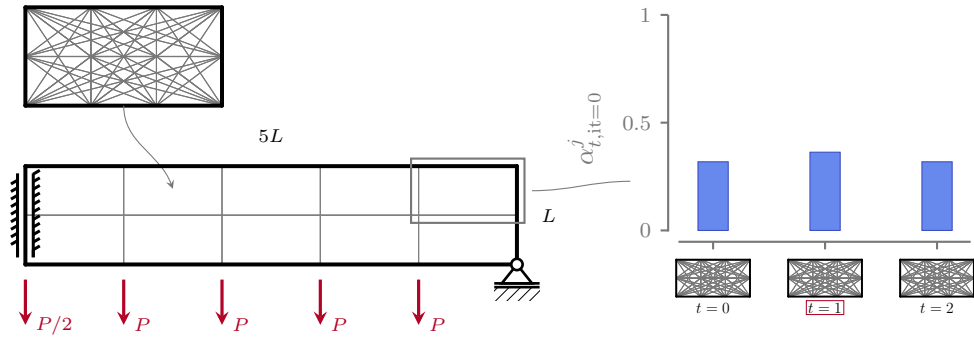


Figure 1.4.

initial ground structure with a uniform cross-sectional area.

Additionally, besides the \bar{n} stress values, we introduce the stress state S for the j -th submodule as:

$$S^j = \sum_{i=0}^{\bar{n}} |\sigma_i^j| \quad (1.10)$$

This addition promotes the clustering not only of submodules loaded in similar ways but also based on similar magnitudes, thereby accounting for variations in voluminous and less voluminous modules.

The full clustering process is depicted in Fig. 1.3, showcasing how the grouping is conducted from the same starting point (FEA-calculated stress distribution on the uniform initial ground structure) but with different numbers of clusters ($N_T = 2, 3$, and 5). Finally, Fig. 1.4 illustrates the initial starting point of the optimization, with a uniform initialization of \bar{a} and the biased weight distribution based on the k-means clustering.

1.2. NUMERICAL APPLICATION

start from here All of the examples presented in this section are solved using the proposed two step formulation, where in the first step we solve a relaxed formulation (no compatibility constraints) to find the optimized modules layout and topology. later, the layout of the modules is fixed, and we solve the optimization problem again to force the structure to comply with the compatibility constraints. The formulations are solved using the non liner interior point solver IPOPT for the two optimization steps

A continuation scheme is set up on the penalization parameter q of the RAMp interpolation scheme used to evaluate the subdomain volume, where the parameter is set up at zero, and then it increase to -0.4 and -0.8 every time the (and the optimizer is not in a restoration phase). The continuation scgheme is implemented only on q as IPOPT is an interior point algorithm, and increasing the p parameter would

put the optimizer well outside of the fesable region everi time the parameter every time it is increased, creating a less than ideal situation. the parameter χ called the cross-sectional area threshold value is set to 1e-4

The stopping criterion used for the Non-Linear Programming (NLP) optimizations is $\|\Delta_{\text{NLP}}\|_\infty \leq \text{tol}_{\text{nlp}}$, with and $\text{tol}_{\text{nlp}} = 10^{-8}$. Δ_{NLP} represents the scaled NLP error, a more comprehensive value used by IPOPT to take into account the optimality of the solution and the constraints violation. The objective function is always scaled so that the initial volume is 1000, the areas are in the interval [0, 100], the initial forces in [0, 100], and the displacement in [0, 100] for the NLP. Several additional parameters are used in the NLP step for cyipopt and IPOPT:

- ▶ `mu_strategy` is set to adaptive
- ▶ `jac_c_constant` is set to yes
- ▶ `num_linear_variables` is set to N , with N equal to the number of bars as the force is linear in this problem
- ▶ `grad_f_constant` is set to yes
- ▶ `linear_solver` is set to pardiso
- ▶ `bound_push` is set to 1e-12
- ▶ `constr_viol_tol` is set to 1e-6
- ▶ `nlp_scaling_method` is set to user-scaling.

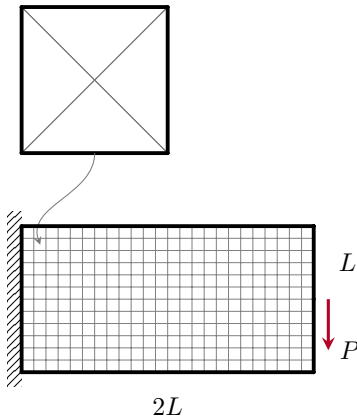


Figure 1.5.: Boundary conditions of the 2D cantilever beam divided in 24x12 subdomains. In the upper part of the image the ground structure of the module composed of $\bar{n} = 6$ elements.

Parameter	Value
L	100
σ_c, σ_t	± 1
P	1
a_{\max}	0.6

Table 1.1.: Material data used for the 2D cantilever beam 2D.

1.2.1. LAYOUT OPTIMIZATION OF FIXED MODULES

The proposed formulation is very versatile and permits to solve very different optimization problem. We start now by optimizing the most simple we can for modular structures. we want to optimize the distribution of a fixed topology cell inside a given domain, and the optimizer should only chose between having the subdomain pouplulated or not. We take a single module topology that is held fixed during the optimization, so $nt=1$ and $\bar{a}_i = 0.6, \forall i$. The only degree of fredoom given to the optimizer is the value of the weight w controlled by the design variable α .

The structure that is optimized is a two dimensional cantilever beam of dimension 200×100 with a center load of magnitude $P = 1$. The optimization domain is partitioned into 24×12 submodules on the x and y axis, respectively. Every subdomain is pouplulated with a simple fully connected 2×2 nodes ground structure with 6 candidate bars as shown in Fig. 1.5 The units of the test case are normalized and a list of the geometry and material parameters is given in Table 1.1. Additionally, in these examples buckling and compatibility constraints are relaxed for simplicity and to preserve the solution simmetry.

Before showing and commenting the optimization results, we presents two boundary cases that allow us to better understand and put into perspective the optimization results. first, we set up a monolithic

optimization with no modular constraints and setting a maximum cross sectional area $a_{\max} = 0.6$. The optimization is performed on the same ground structure shown in Fig. 1.5. This results should represent the lower bound of the optimization, representing the minimum value at which modular optimization should tend, the closer to this value, the better. The resulting topology shows a volume $V = 832.848$ and a topology that resembles the one obtained in classic topology optimization. Secondly, we present a fully modular structure, in which all the subdomains present the topology of the fixed topology module with all bars set to 0.6. In that case the structure shows a volume $V = 9832.935$ and it represents the upper bound for the optimization. The topology of the fully modular structure is shown in Fig. 1.7.

Now that we have set up the reference for better understand the optimization results, we perform the optimizations of the layout of the fixed topology module. Just for the first example we decided not to penalize intermediate weights, so $p = q = 0$ and then $w = \alpha$. The optimized structure topology is shown in Fig. 1.8a and Fig. 1.8b, in which we show also the weight distribution of the solution. At this stage, the optimized structure shows a volume $V = 1567.216$, a value that is not that far from the monolithic reference. However, this solution is non physical as many subdomains present intermediate weights (see the weight distribution in Fig. 1.8c) and we need to threshold the result. The thresholding value is set to 0.01, so any subdomains that have a weight w less than this value is considered empty. The result of the thresholding is presented in Fig. 1.8d, in which we see that all weights that are present are now set to 1. The resulting structure has a volume $V = 8808.671$, a very noticeable increase due to the high number of intermediate weights shown by the solution of Fig. 1.8b.

To solve this problem, we set up a multi-phase RAMP interpolation where we simultaneously penalize mechanical properties (using the parameter p) and we artificially increase the volume (using the parameter q) of modules with intermediate weights. In this optimization we set $p = 8$ and $q_{\min} = -0.8$, and a continuation scheme is used on the q parameter to gradually decrease it to the minimum value as already explained in Section 1.2. The optimized structure topology with penalized intermediate weights is shown in Fig. 1.8e and Fig. 1.8f and it has a volume $V = 1961.175$, a 25 % volume increase with respect to the unpenalized structure. However we can clearly see how this solution presents way less subdomains with intermediate weight and this is very reflected after the thresholding phase shown in Fig. 1.8g, in which the volume is now $V =$, more than 60 % less than the unpenalized structure. The difference between the structure of Fig. 1.8f and Fig. 1.8g could also be less, as in this case we see that the subdomains creates beams that are made by only an element and it is enough to transfer the loads. A finer subdivision of the initial structure could

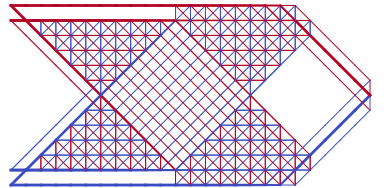


Figure 1.6.: $V = 832.848$

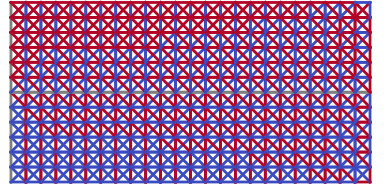


Figure 1.7.: $V = 9832.935$

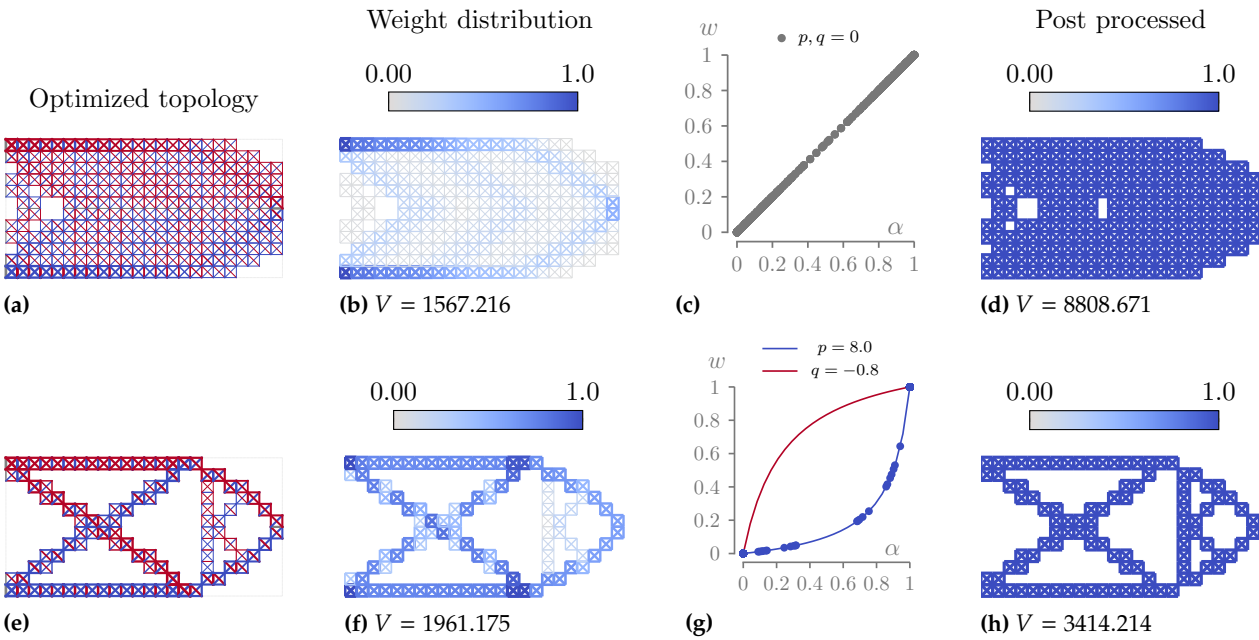


Figure 1.8.

then beneficial.

6. Bendsøe et al. (1999), 'Material interpolation schemes in topology optimization'
7. Sigmund et al. (2016), 'On the (non-)optimality of Michell structures'

Similarities with classic topology optimization. [6, 7]

Now that we assessed the need for a penalization scheme, we test the proposed optimization formulation with some test cases using multiple fixed modules. As the topology of the module (\bar{a}) is not modified, no perturbation is done on the initial starting point and alpha at iteration 0 is set to $\alpha = 0.5$, $\forall j, t$. First test we performed was to optimize the layout of two different modules ($N_T=2$) that present the same cell topology connectivity but different cross-sectional areas. we used two 2-nodes fully connected modules with uniform coss sectional areas set to 0.6 and 0.2, to simulate high and low densities modules for hig and low stress part of the structure. The results are presented in Fig. 1.9a and b and the structure optimized present a volume $V = 2987.437$. This represent a 12 % improvement over the single fixed topology.

Similar results are presented in Fig. 1.9c and d, in which we optimize the module layout of two modules that present a different mirrored topology (see Fig. 1.9d). The structure optimized in this way shows a very different module layout and a final volume $V = 2317.462$, even better than before. These two examples confirming that giving more design freedom to the optimizer can improve the mechanical performance of the modular structure..

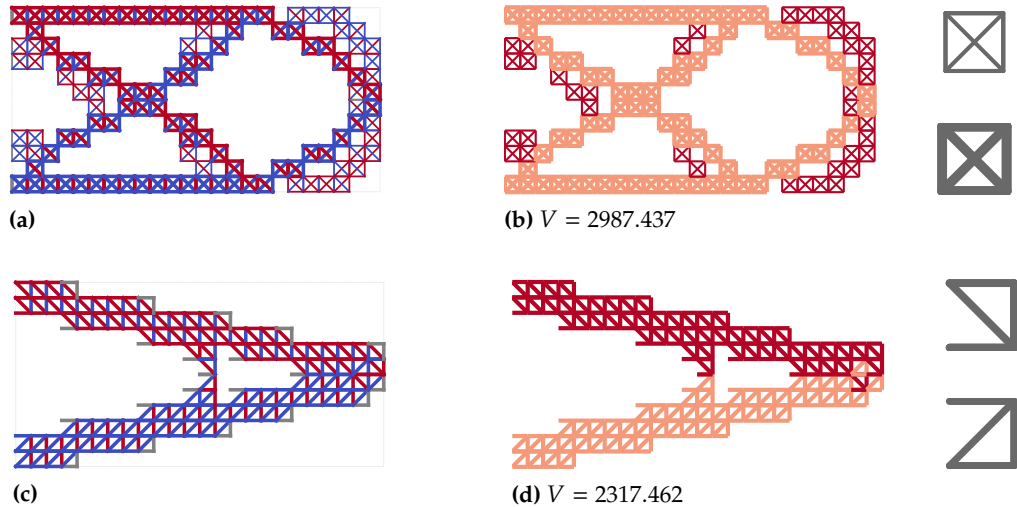


Figure 1.9.

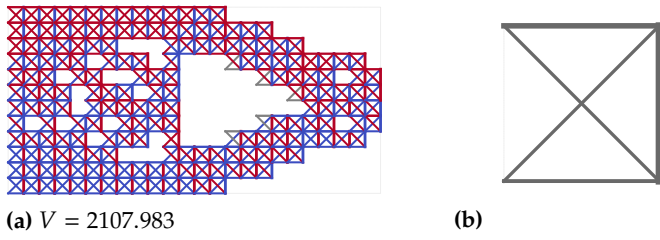


Figure 1.10.

1.2.2. MODULES AND LAYOUT OPTIMIZATION

We now optimize a modular structure using multiple modules that can now vary their topology (the values of \bar{a}_{bar} are no longer fixed). In the case of $nt=1$, the starting point for the value of α is still trivial ($\alpha=1$ for all) and the structure we obtain together with the optimized module topology is shown in Fig. 1.10a and b. The modular structure has a volume $V = 2107.983$, the best found until this point and confirming the interest in optimizing both the modules topology and layout.

moving now to the layout and topology optimization of modular structures with a number of module topologies $N_T > 1$, there is the need to use the k-means clustering to evaluate the starting point for the layout module variable α . A FEA is set up on the original ground structure with uniform cross-sectional areas and the k-means clustering is performed over the stress distribution using N_T different clusters. The process is shown for example for $nt=2$ and $nt=5$ on Fig. 1.11, in which we see that in general we have the clusters following more and less stressed zones especially in the $nt=2$ example. But it is only when the number of clusters reaches 5 that we start to see a difference between tension and compression, with a symmetrical solution with respect to the neutral axis of the beam.

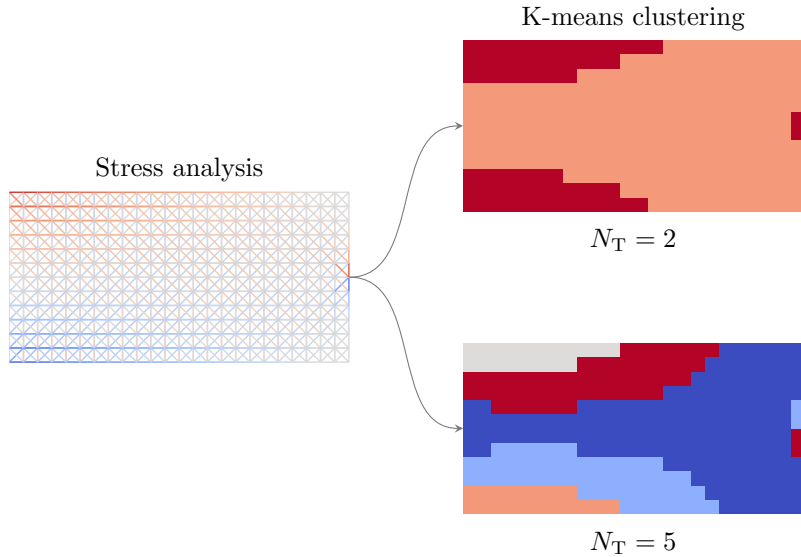


Figure 1.11.

Table 1.2.

N_T	1	2	3	4	5
N_{sub}	288	288	288	288	288
$N_{\text{sub,e}}$	107	45	72	43	50
V	2107.983	1722.61	1730.05	1589.90	1416.05
a_{\max}	0.37	0.35	0.48	0.54	0.53
φ	17.16 %	17.86 %	14.20 %	17.95 %	16.65 %
ψ	0.52	0.59	0.57	0.61	0.67
t	35 s	18 s	14 s	17 s	26 s

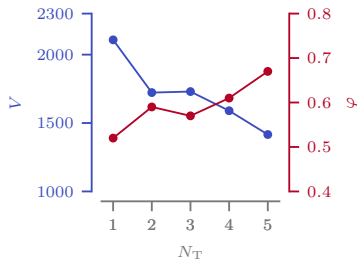


Figure 1.12.

Starting from the advised starting point from the kmeans cludtering, the optimization are performed for nt from 2 to 5, and their results are resumed in the Table 1.2. Here are the main takeawqys : Having a look at the evolution of the volume of the optimized structures with the different number of modules nt, we notice how they behave like expected as a monotonic descending function. This behaviour could be explained by in general a major specificity of the modules that chan shape their topology to more specific load cases and be less general purpose. We can see effettivamente that the value of the average bar load is increasing with the number of module topologies. This ehaviour is resumed in Fig. 1.12. Additionally it is interesting how, increasing the number of module topologies the number of empty subdomains drop from 107 and stabilize at around 50, suggesting that for this specific test case more modules topologies are employed, the number of empty subdomains decrease, showing that it is better to have many light modules and not few stron and heavy ones. Finally, concerining the calculation time, we see no real correlation between the number of modules. We speculate that THis is because, even if the number of design variables increase, the problem is often easier to solve and less iterations are necessary to attain convergence. The topology of the modular structure with nt=2 e nt=5 is showed togheter whit theri optimized modules in Fig. 1.13. It is interesting to notice how the optimized structures shows similar modules layout with

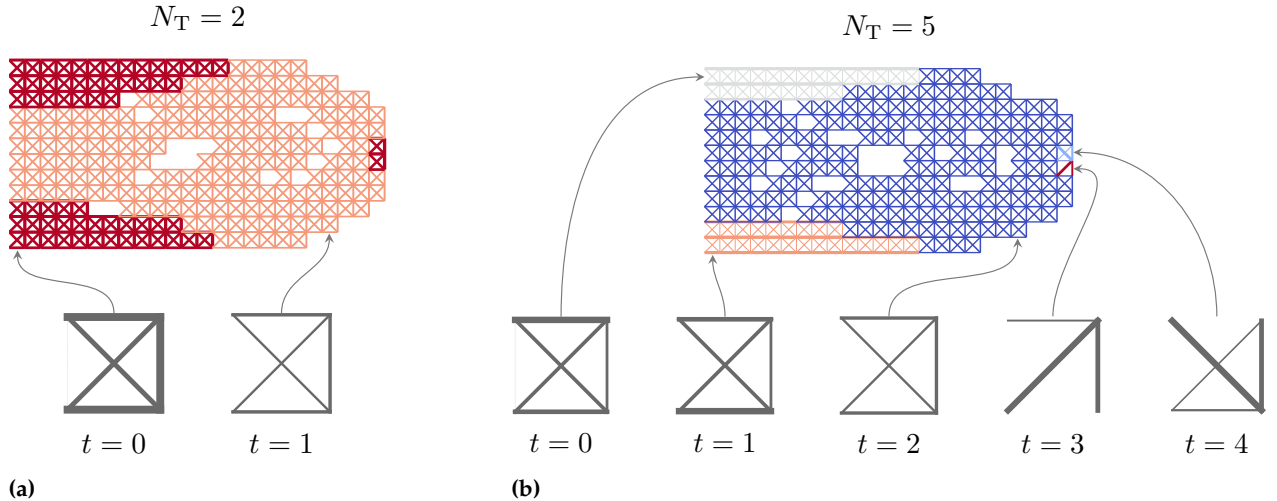


Figure 1.13.

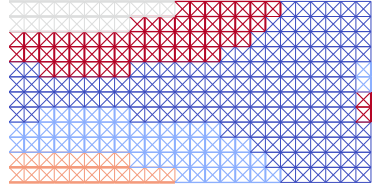
respect to the number of module topology.

last thing we want to comment on is a comparison betweenn the optimized structure with $nt=5$ of Fig. 1.13b and the structure we would obtain if we used the clustering algo suggested structure layout to set the mapping matrix H and the variable linking algorithm described in Section ???. Using this formulation, the layout of the structure is fixed and no changes or empty modules are possible. The optimized structure using this algorithm is shown in Fig. 1.14 and it has a volume $V = 1727.314$, more than 20 % more with respect to the proposed method slution. the differnece can be explained by two factors: forst the proposed formulation permits to have empty subdomains, and this definetly helps for lightening the structure. secondly, the proposed formulation uses the clustering results only as a starting point for the layout of the optimization, but the layout can then evolve.

1.2.3. A BENCHMARK CASE STUDY: A SIMPLY SUPPORTED MODULAR BRIDGE

The proposed formulation and solution algorithm is now benchmarked against what we find in the literatire. To the knowledge of the authors, there is no other works that optimize layout and topology of modular structures using a gradient descent algorithm and continuous design variables. However, we can find som similar results obtained using MILP algorithm or simulated annealing to optimize modular structure. This is the case for example of the works of Tugilimana [8, 9] and we will now compare the restults.

The considered structure is a modular structure based on the Bailey bridge [11], a concept that has been studied for military puropses and used also for civil applications e.g. temporary bridge structures, thanks adaptability, low weight, but especially extremely fast erection

Figure 1.14.: $V = 1727.314$

8. Tugilimana et al. (2017), 'Spatial orientation and topology optimization of modular trusses'

9. Tugilimana et al. (2019), 'An integrated design methodology for modular trusses including dynamic grouping, module spatial orientation, and topology optimization'



Figure 1.15.: Bailey bridge placed on construction site road over Orava river (Slovakia) [10].

11. Department of the Army (1986), 'Field Manual No. 5-277, Panel Bridge, Bailey Type, Washington DC.'

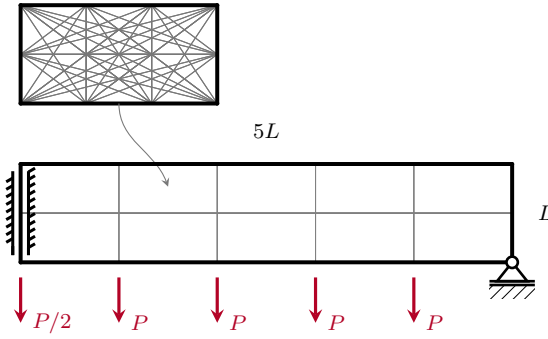


Figure 1.16.

and almost immediate usability for traffic are utilized (see Fig. 1.15). The structure is 20 modules long and 2 modules high, each module is 3.050 m long (10 ft) and 1.525 m high (5 ft), resulting in a total bridge span of 30.50 m (100 ft). The load case is represented in Fig. 1.16, together with the geometrical and material data (normalized) used for the optimization in Table 1.3. We optimize here only the symmetric part. In this load case we consider all the constraints of the formulation ?? but the buckling, as Tugilimnana did.

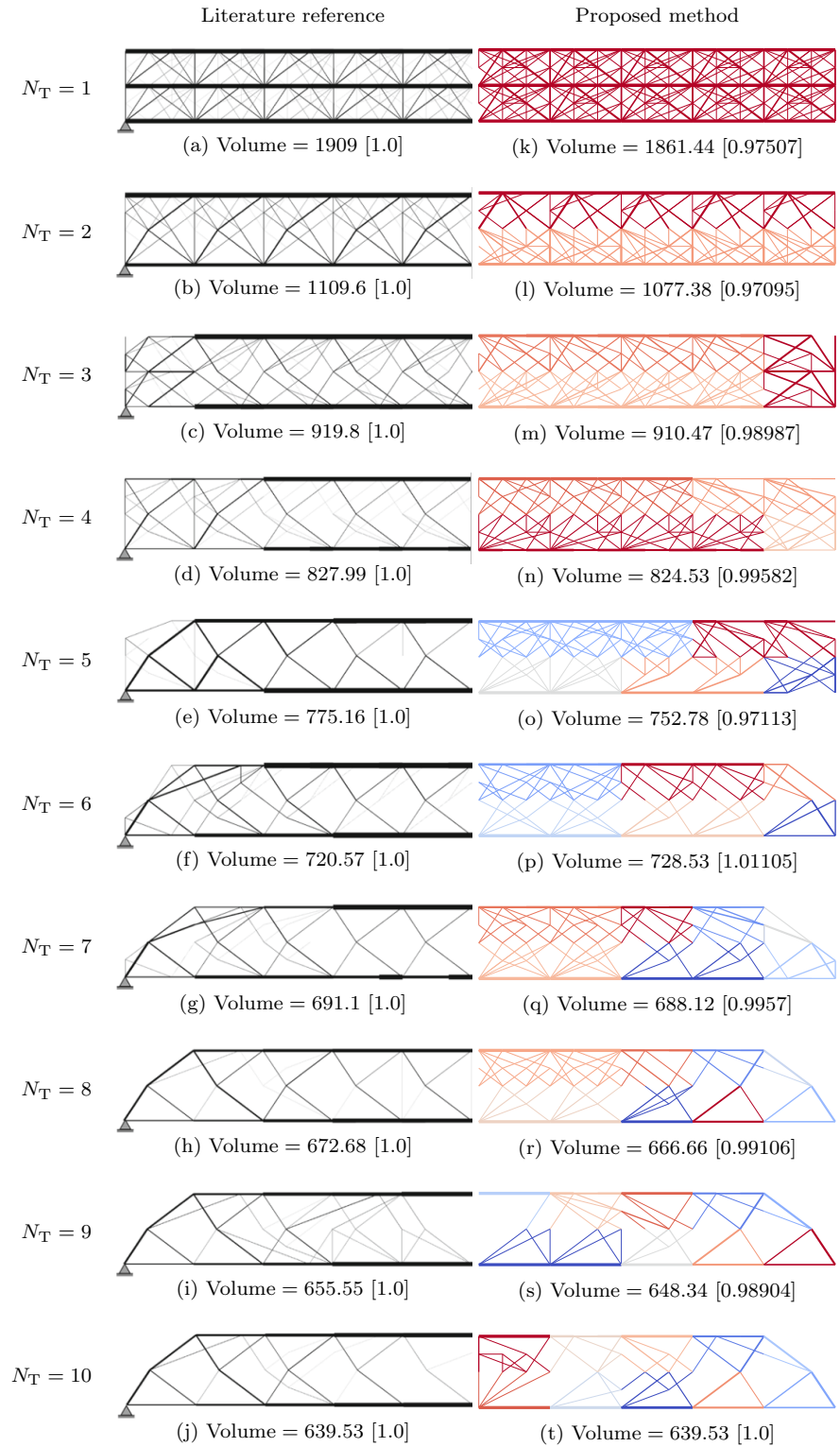
Parameter	Value
L	3.05
σ_c, σ_t	± 1
P	1

Table 1.3.: Material data used for the

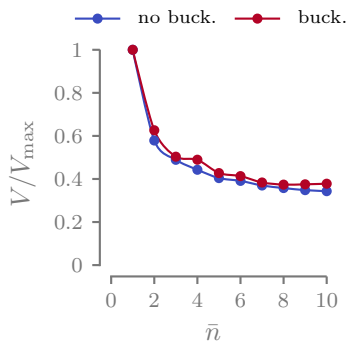
9. Tugilimana et al. (2019), 'An integrated design methodology for modular trusses including dynamic grouping, module spatial orientation, and topology optimization'

The resulting optimized structures are presented in the right part of Fig. 1.17, together with the topology of the structures optimized by Tugilimana *et al.* [9]. Below every subfigure it is present the structure volume and, in square brackets, the relative value with respect to the Tugilimana solution. Even if the reference images do not highlight the submodules that show the same module topology, we see that the module layout is not always the same e.g. in the case of $N_T = 4$ or $N_T = 5$. We notice that the proposed optimization algorithm is not only capable of optimizing an intrinsically discrete optimization problem using continuous design variables and a gradient based optimizer, but also to improve the results found in the literature up to 3 %. The structure obtained with $n_t=10$ is exactly the same we would obtain by optimizing the structure if we did not consider the modular constraints.

Up until now we used always normalized material data and dimensions and we never considered local buckling of truss. We test for that reason what happens in this very load case if we do that, and we are very interested in seeing if these changes affect a lot the modules topology and layout in the structure. The material data used for the optim is presented in Table 1.4 and represent an aluminium. The cross sections are supposed circular for the local buckling evaluation. The topological buckling is taken into account inside the modules as already explained in Section ??.

**Figure 1.17.**

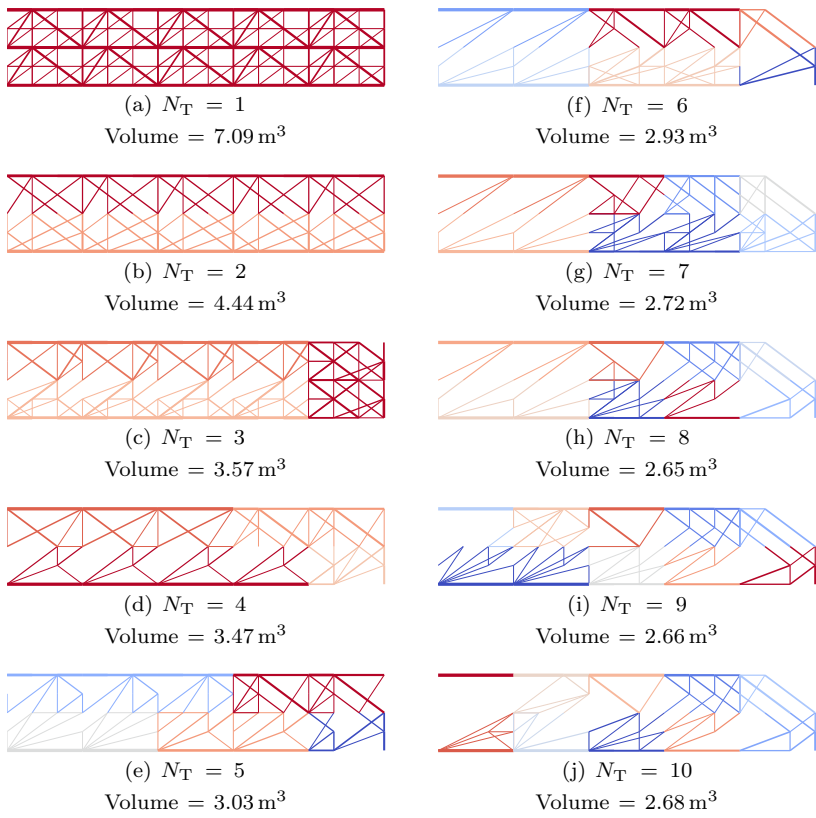
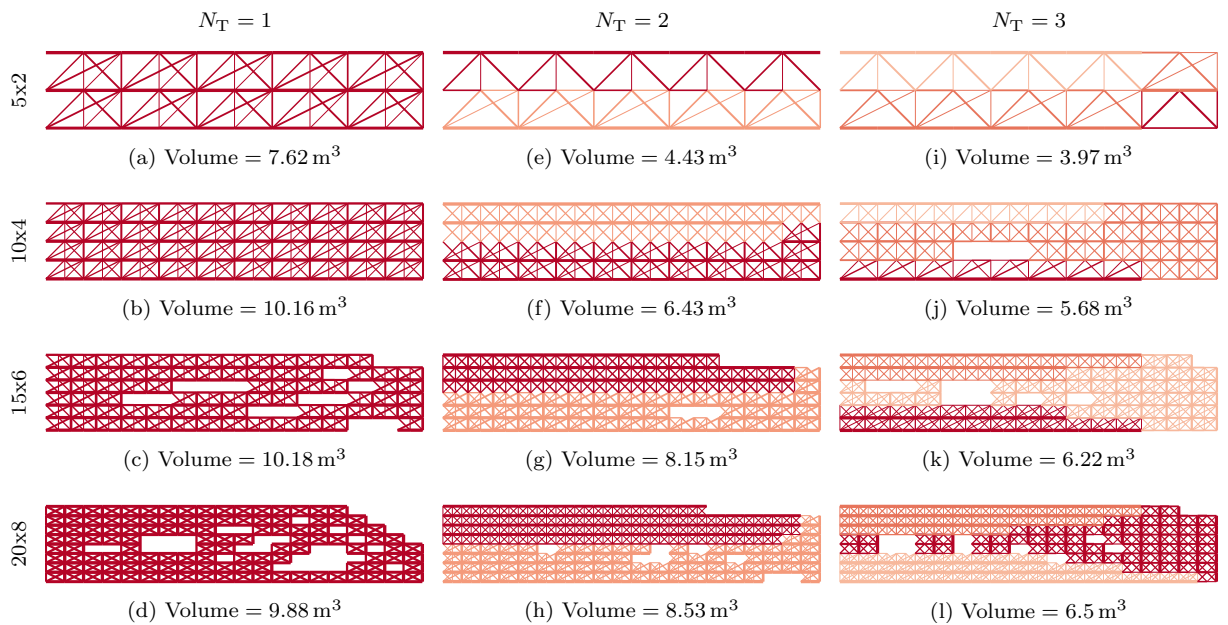
Parameter	Value
L	3.05 m
E	69 GPa
σ_c, σ_t	± 270 MPa
P	1 MN

Table 1.4.: Material data used for the**Figure 1.18.**

The optimized structure for the Bailey bridge with buckling constraints are shown for a different number of module topologies in Fig. 1.19. quickly comparing them with the results without the buckling we notice that for this test case the layout of the modules is the same. The topology however is very different with in general a little bit less active bars. The volume can be directly compared, so we normalize them and plot them on Fig. 1.18, showing that adding multiple module topologies is beneficial in the same exact way with or without buckling constraints. We can also comment that the biggest reduction on the volume from the inclusion of additional modules come especially at the beginning, e.g. going from $n_t=1$ to $n_t=2$ or from $n_t=2$ to $n_t=3$, while the difference at higher numbers is marginal as the succession show a plateau.

willing to explore how the different parameters can influence the results, the topology and the layout, we test the same load case with a different number of subdomains and modules. We use the very same test case, with the only difference that we are now using a 3x2 nodes ground structure for having faster calculation times.

Commenta volume, di come Influence of the number Fig. 1.21 of subdomains on the volume of the steep increase and then plateau, different from before optimized modular structure cambia e non sale piu in maniera ma si stoppa a un plateau principalmente due motivi, cambia il metodo di rottura, non piu buckling e passo a stress e poi ho i vuoti. we observe that when we have not many subdomains the structure is always all filled, with no empty subdomains. but with the increasing number of subdomains we notice more and more empty subdomains, helping to keep the structure light.

**Figure 1.19.****Figure 1.20.**

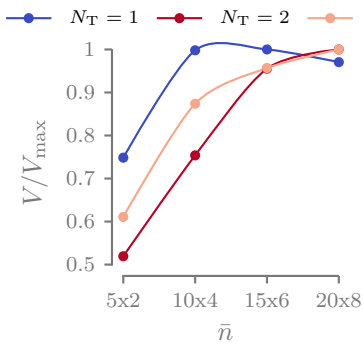


Figure 1.21.

last thing commenta per esempio imm d in cui cambia il modo di rottura e la cell è simmetrica in compressione e in tensione. molto efficace uso del materiale in questa maniera e quindi il volume scende.

1.2.4. SIMPLY SUPPORTED 3D BEAM

The last test we conduct is on the simply supported 3d beam, a load case introduced in Chapter ?? and used tout au long de cette these. we rappel the test case and the material and geometric data used for the optimization process in Fig. 1.22 and Table 1.5. as already done we optimize here only one forth of the entire structure thanks to its symmetry planes. we conduct the optimization using 6x2x3 subdomains on the X, Y and Z axis respectively and every module is discretized using a 3x3x3 fully connected ground structure ($\bar{n} = 351$). The optimization is conducted using three different number of modules, $N_T=1,2,3$.

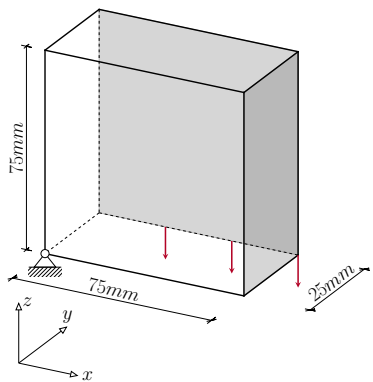


Figure 1.22.: Symmetric boundary conditions of the simply supported 3D beam. In gray are the symmetry planes of the test case.

The resulting optimized structures are presented in Fig. 1.23 and the associated numerical results are presented in Table 1.6. The first thing we notice is that in this specific test case the optimizer converges to solutions where the sum of alpha for every subdomains is always equal to one. while before we have seen that the formulation arrived at create empty subdomains where the sum of alpha is zero, here the optimizer failed. the empty subdomains of the nt=2 and nt=3 corresponds to cases where the topology of one module is set to zero and the optimizer put the value of the corresponding alpha to one. In this way the solution is still optimized correctly, but using a module topology en plus e.g. looking at Fig. 1.23b and e, so the solution for nt=2, we see that the optimized structure shows only one module topology, the other being the empty one.

we speculate that this problem come from the optimizer's settings used to normalize the design variables and the constraint for the optimization. we found that for example even if we scaled the alpha variable and the corresponding constraints in multiple values, we still got the same results. This problem suggest us that even if the starting point perturbation definetly helps achieving a good optiized structure, more work has to be done on developing a new resolution strategy, maybe trying to separate the topology and layout variables and solving iteratively the two problem separated one iteration at a time.

Even having this problem we can however notice having a look at the volume V and the mean densities $\bar{\rho}$ of Table 1.6 how the modular structures with nt=2 and nt=3 reaches very similar values to the monolithic reference ($n_{sub} = 1$) shown in Fig. 1.24, while being modular.

Table 1.5.: Material data used for the simply supported 3D beam optimization.

Parameter	Value
E	2.7 GPa
σ_c, σ_t	± 55 MPa
ρ	1.14 g cm^{-3}
P	100 N

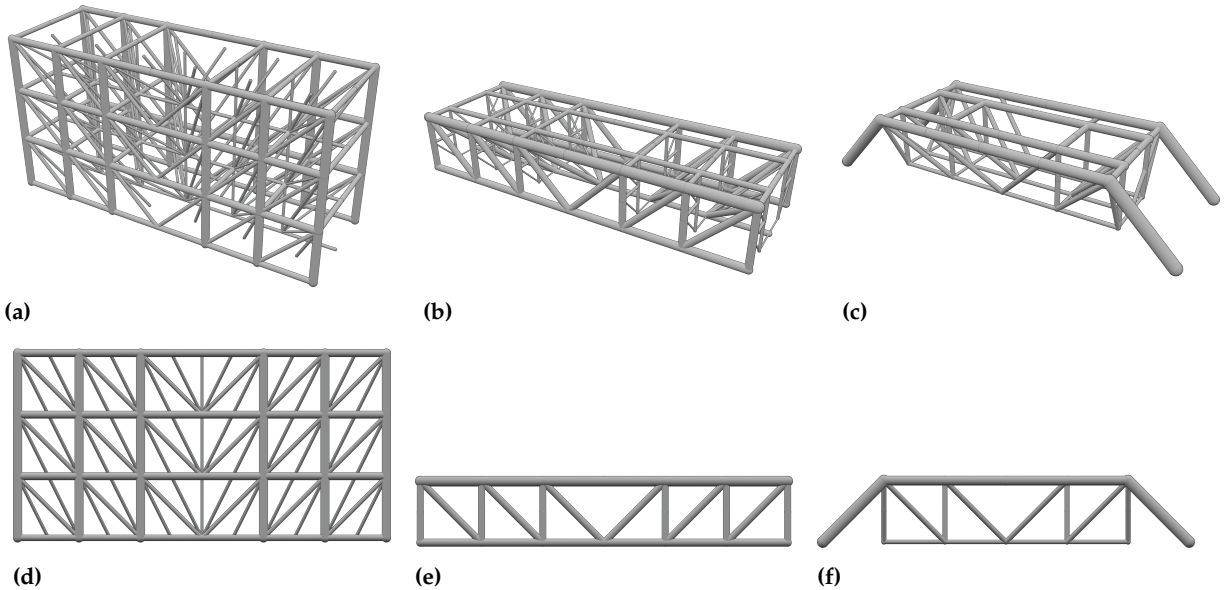
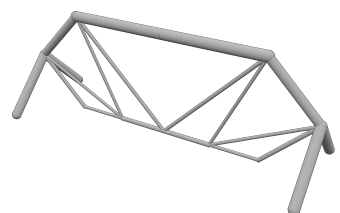


Figure 1.23.

N_T	-	1	2	3
N_{sub}	1	36	36	36
$N_{\text{opt}} (N_{\text{el}})$	20 (1984)	360 (12636)	204 (12636)	104 (12636)
$V [\text{cm}^3]$	9.907	27.958	15.548	10.178
$V [\%]$	1.761	4.970	2.764	1.809
$\bar{\rho} [\text{kg/m}^3]$	80.31	226.65	126.05	82.51
$C [\text{J}]$	3.71	5.20	6.21	4.141
$a_{\max} [\text{mm}^2]$	37.61	9.40	12.81	15.81
φ	100.00 %	21.11 %	39.21 %	80.77 %
ψ	1.00	0.47	0.66	0.87
t	4 s	1 m 18 s	42 s	10 m 22 s

Table 1.6.

Figure 1.24.: Perspective view of the monolithic simply supported 3D beam optimized structure with $V = 9.907 \text{ cm}^3$

1.3. CONCLUSION

in this chapter we presented an innovative optimization formulation that optimize the structural volume of modular structures. The solving algorithm takes advantages of the physical informations of the model, exploiting the analytical derivatives, and uses a gradient descent optimization algorithm. The discrete categorical variables used to choose the module layout are modeled using a weighted sum of continuous weights, that fits the optimization scheme, and a double penalization scheme is proposed to reduce the appearance of non physical intermediate weights. The proposed formulation is tested over a multitude of test cases, two and three dimensional, from the literature or innovative. These test assessed that the use of this optimization formulation helps the modular structures to achieve volumes that are really near the ones from monolithic optimization, all being modular, offering a good tradeoff between optimality and manufacturing complexity. However, up until now we concentrated

only on dummy test cases that are not of an engineering relevance. for that reason, in the next chapter we address this problem by focussing on the application of the presented optimization formulations in the aerospace context.

BIBLIOGRAPHY

- [1] Sigmund, Ole, 'On the usefulness of non-gradient approaches in topology optimization', *Structural and Multidisciplinary Optimization* 43.5 (May 2011), pp. 589–596.
DOI: [10.1007/s00158-011-0638-7](https://doi.org/10.1007/s00158-011-0638-7) cited on page 1
- [2] Stegmann, J. and Lund, E., 'Discrete material optimization of general composite shell structures', *International Journal for Numerical Methods in Engineering* 62.14 (Apr. 2005), pp. 2009–2027.
DOI: [10.1002/nme.1259](https://doi.org/10.1002/nme.1259) cited on page 1
- [3] Stolpe, M. and Svanberg, K., 'An alternative interpolation scheme for minimum compliance topology optimization', *Structural and Multidisciplinary Optimization* 22.2 (Sept. 2001), pp. 116–124.
DOI: [10.1007/s001580100129](https://doi.org/10.1007/s001580100129) cited on page 2
- [4] Hvejsel, Christian Frier and Lund, Erik, 'Material interpolation schemes for unified topology and multi-material optimization', *Structural and Multidisciplinary Optimization* 43.6 (June 2011), pp. 811–825.
DOI: [10.1007/s00158-011-0625-z](https://doi.org/10.1007/s00158-011-0625-z) cited on page 2
- [5] Bakker, Coen, Zhang, Lidan, Higginson, Kristie, and Keulen, Fred van, 'Simultaneous optimization of topology and layout of modular stiffeners on shells and plates', *Structural and Multidisciplinary Optimization* 64.5 (Nov. 2021), pp. 3147–3161.
DOI: [10.1007/s00158-021-03081-0](https://doi.org/10.1007/s00158-021-03081-0) cited on page 6
- [6] Bendsøe, M. P. and Sigmund, O., 'Material interpolation schemes in topology optimization', *Archive of Applied Mechanics* 69.9 (Nov. 1999), pp. 635–654.
DOI: [10.1007/s004190050248](https://doi.org/10.1007/s004190050248) cited on page 10
- [7] Sigmund, Ole, Aage, Niels, and Andreassen, Erik, 'On the (non-)optimality of Michell structures', *Structural and Multidisciplinary Optimization* 54.2 (Aug. 2016), pp. 361–373.
DOI: [10.1007/s00158-016-1420-7](https://doi.org/10.1007/s00158-016-1420-7) cited on page 10
- [8] Tugilimana, Alexis, Thrall, Ashley P., Descamps, Benoît, and Coelho, Rajan Filomeno, 'Spatial orientation and topology optimization of modular trusses', *Structural and Multidisciplinary Optimization* 55.2 (Feb. 2017), pp. 459–476.
DOI: [10.1007/s00158-016-1501-7](https://doi.org/10.1007/s00158-016-1501-7) cited on page 13
- [9] Tugilimana, Alexis, Coelho, Rajan Filomeno, and Thrall, Ashley P., 'An integrated design methodology for modular trusses including dynamic grouping, module spatial orientation, and topology optimization', *Structural and Multidisciplinary Optimization* 60.2 (Aug. 2019), pp. 613–638. cited on pages 13, 14

- cited on page 13
- [10] Prokop, Jozef, Odrobiňák, Jaroslav, Farbák, Matúš, and Novotný, Vladimír, 'Load-Carrying Capacity of Bailey Bridge in Civil Applications', *Applied Sciences* 12.8 (Jan. 2022), Number: 8 Publisher: Multidisciplinary Digital Publishing Institute, p. 3788.
DOI: [10.3390/app12083788](https://doi.org/10.3390/app12083788)
- cited on page 13
- [11] Department of the Army, 'Field Manual No. 5-277, Panel Bridge, Bailey Type, Washington DC.' 1986

APPENDIX

SENSITIVITY ANALYSIS OF THE MODULAR STRUCTURE OPTIMIZATION ALGORITHM

A

SENSITIVITY ANALYSIS

COMMON DERIVATIVES

$$\frac{\partial \mathbf{a}^j}{\partial \bar{\mathbf{a}}_t} = w_t^j \quad (\text{A.1})$$

$$\frac{\partial \mathbf{a}^j}{\partial \alpha_t^j} = \frac{\partial \mathbf{a}^j}{\partial w_t^j} \frac{\partial w_t^j}{\partial \alpha_t^j} \quad (\text{A.2})$$

$$\frac{\partial \mathbf{a}^j}{\partial w_t^j} = \bar{\mathbf{a}}_t \quad (\text{A.3})$$

$$\frac{\partial w_t^j}{\partial \alpha_t^j} = \frac{1 + (\cdot)}{(1 + (\cdot))(1 - \alpha_t^j)^2} \quad (\text{A.4})$$

where (\cdot) is either equal to p or q .

$$\frac{\partial^2 w_t^j}{\partial (\alpha_t^j)^2} = \frac{2(\cdot)(1 + (\cdot))}{(1 + (\cdot))(1 - \alpha_t^j)^3} \quad (\text{A.5})$$

VOLUME JACOBIAN

$$\frac{\partial V}{\partial \bar{\mathbf{a}}_t} = \bar{\ell}^T \sum_{j=1}^{N_{\text{sub}}} \tilde{w}_t^j, \text{ with } t \in [1, \dots, N_T] \quad (\text{A.6})$$

$$\frac{\partial V}{\partial \alpha_t^j} = \frac{\partial V}{\partial w_t^j} \frac{\partial w_t^j}{\partial \alpha_t^j} \quad (\text{A.7})$$

$$\frac{\partial V}{\partial w_t^j} = \bar{\ell}^T \bar{\mathbf{a}}_t \quad (\text{A.8})$$

$$\frac{\partial V}{\partial q} = 0 \quad (\text{A.9})$$

$$\frac{\partial V}{\partial U} = 0 \quad (\text{A.10})$$

VOLUME HESSIAN

$$\frac{\partial^2 V}{\partial \bar{a}_t \partial \alpha_t^j} = \bar{\ell}^T \frac{\partial \tilde{w}_t^j}{\partial \alpha_t^j} \quad (\text{A.11})$$

$$\frac{\partial^2 V}{\partial (\alpha_t^j)^2} = \bar{\ell}^T \bar{a}_t \frac{\partial^2 w_t^j}{\partial (\alpha_t^j)^2} \quad (\text{A.12})$$

$$\frac{\partial^2 V}{\partial \bar{a}_t^2} = 0 \quad (\text{A.13})$$

EQUILIBRIUM JACOBIAN

$$g_{\text{eq}} := Bq = f \quad (\text{A.14})$$

Not impacted by the clustering of the variables.

$$\frac{\partial g_{\text{eq}}}{\partial \alpha} = 0 \quad (\text{A.15})$$

STRESS CONSTRAINTS TENSION JACOBIAN

$$g_t := q - \sigma_t a \leq 0 \quad (\text{A.16})$$

$$\frac{\partial g_t^j}{\partial \bar{a}_t} = \frac{\partial g_t^j}{\partial a^j} \frac{\partial a^j}{\partial \bar{a}_t} \quad (\text{A.17})$$

$$\frac{\partial g_t^j}{\partial a^j} = -\sigma_t \quad (\text{A.18})$$

$$\frac{\partial g_t^j}{\partial \bar{a}_t} = -\sigma_t w_t^j \quad (\text{A.19})$$

$$\frac{\partial g_t^j}{\partial \alpha^j} = \frac{\partial g_t^j}{\partial a^j} \frac{\partial a^j}{\partial \alpha^j} \quad (\text{A.20})$$

STRESS CONSTRAINTS TENSION HESSIAN

$$\frac{\partial^2 g_t^j}{\partial \bar{a}_t \partial \alpha_t^j} = -\sigma_t \frac{\partial w_t^j}{\partial \alpha_t^j} \quad (\text{A.21})$$

$$\frac{\partial^2 g_t^j}{\partial (\alpha_t^j)^2} = -\sigma_t \bar{a}_t \frac{\partial^2 w_t^j}{\partial (\alpha_t^j)^2} \quad (\text{A.22})$$

BUCKLING JACOBIAN

$$g_b := q \frac{s \mathbf{a}^2}{\ell^2} \geq 0 \quad (\text{A.23})$$

$$\frac{\partial g_b^j}{\partial \mathbf{a}^j} = 2 \frac{s \mathbf{a}^j}{\ell^2} \quad (\text{A.24})$$

$$\frac{\partial g_b^j}{\partial \bar{\mathbf{a}}_t} = \frac{\partial g_b^j}{\partial \mathbf{a}^j} \frac{\partial \mathbf{a}^j}{\partial \bar{\mathbf{a}}_t} \quad (\text{A.25})$$

$$\frac{\partial g_b^j}{\partial \bar{\mathbf{a}}_t} = 2 \frac{s \mathbf{a}^j}{\ell^2} w_t^j \quad (\text{A.26})$$

$$\frac{\partial g_b^j}{\partial \alpha^j} = \frac{\partial g_b^j}{\partial \mathbf{a}^j} \frac{\partial \mathbf{a}^j}{\partial \alpha^j} \quad (\text{A.27})$$

$$\frac{\partial g_b^j}{\partial \alpha_t^j} = 2 \frac{s \mathbf{a}^j}{\ell^2} \bar{\mathbf{a}}_t \frac{\partial w_t^j}{\partial \alpha_t^j} \quad (\text{A.28})$$

$$\frac{\partial g_b^j}{\partial \alpha_t^j} = 2 \frac{s \mathbf{a}^j}{\ell^2} \bar{\mathbf{a}}_t \frac{1 + (\cdot)}{\left(1 + (\cdot)(1 - \alpha_t^j)\right)^2} \quad (\text{A.29})$$

BUCKLING HESSIAN

$$\frac{\partial^2 g_b^j}{\partial \bar{\mathbf{a}}_l \partial \alpha_m^j} = 2 \frac{s}{\ell^2} w_l^j \frac{\partial \mathbf{a}^j}{\partial \alpha_m^j} + 2 \frac{s \mathbf{a}^j}{\ell^2} \frac{\partial w_l^j}{\partial \alpha_m^j} \quad (\text{A.30})$$

$$\frac{\partial^2 g_b^j}{\partial \bar{\mathbf{a}}_l \partial \alpha_m^j} = 2 \frac{s}{\ell^2} w_l^j \frac{\partial w_m^j}{\partial \alpha_m^j} \bar{\mathbf{a}}_m + 2 \frac{s \mathbf{a}^j}{\ell^2} \frac{\partial w_l^j}{\partial \alpha_m^j} \quad (\text{A.31})$$

$$\frac{\partial^2 g_b^j}{\partial \bar{\mathbf{a}}_l \partial \alpha_m^j} = \begin{cases} 2 \frac{s}{\ell^2} \frac{\partial w_l^j}{\partial \alpha_t^j} \left(w_t^j \bar{\mathbf{a}}_t + \mathbf{a}^j \right) & \text{if } l = m = t \\ 2 \frac{s}{\ell^2} w_l^j \frac{\partial w_m^j}{\partial \alpha_m^j} \bar{\mathbf{a}}_m & \text{otherwise.} \end{cases} \quad (\text{A.32})$$

$$\frac{\partial^2 g_b^j}{\partial \bar{\mathbf{a}}_l \partial \bar{\mathbf{a}}_m} = 2 \frac{s}{\ell^2} w_l^j w_m^j \quad (\text{A.33})$$

$$\frac{\partial^2 g_b^j}{\partial \alpha_l^j \partial \alpha_m^j} = 2 \frac{s}{\ell^2} \bar{\mathbf{a}}_l \frac{\partial \mathbf{a}^j}{\partial \alpha_m^j} \frac{\partial w_l^j}{\partial \alpha_l^j} + 2 \frac{s \mathbf{a}^j}{\ell^2} \bar{\mathbf{a}}_l \frac{\partial^2 w_l^j}{\partial \alpha_l^j \partial \alpha_m^j} \quad (\text{A.34})$$

$$\frac{\partial^2 \mathbf{g}_b^j}{\partial \alpha_l^j \partial \alpha_m^j} = \begin{cases} 2 \frac{s}{t^2} \bar{\mathbf{a}}_t^2 \left(\frac{\partial w_t^j}{\partial \alpha_t^j} \right)^2 + 2 \frac{s a_t^j}{t^2} \bar{\mathbf{a}}_t \frac{\partial^2 w_t^j}{\partial (\alpha_t^j)^2} & \text{if } l = m = t \\ 2 \frac{s}{t^2} \bar{\mathbf{a}}_l \bar{\mathbf{a}}_m \left(\frac{\partial w_m^j}{\partial \alpha_m^j} \right) \left(\frac{\partial w_l^j}{\partial \alpha_l^j} \right) & \text{otherwise.} \end{cases} \quad (\text{A.35})$$